Innovations in Systems and Software Engineering
https://doi.org/10.1007/s11334-021-00414-6

S.I. : MULTIFACETED INTELLIGENT COMPUTING SYSTEMS (MICS)

A hybrid approach for water body identification from satellite images using NDWI mapping and histogram of gradients

Tanmoy Halder[1] · Debasish Chakraborty[3] · Ramen Pal[2] · Sunita Sarkar[2] · Somnath Mukhopadhyay[2] · Nishtha Roy[2] · Sunil Karforma[4]

Received: 7 June 2021 / Accepted: 9 October 2021

Abstract
Application of different water identification indices and their modified form with a threshold is a common practice in surface water identification from multispectral images. Implementation of the statistical features of water present in such images to improve the accuracy of existing approaches is a novel application. A dynamic threshold selection is more suitable for the detection of sediment–water. In consideration of the facts, the present study proposed a hybrid approach for automatic surface water detection. Fuzzy c-means, NDWI, and a statistical feature: gradient are used to classify and therefore identify surface water. The study area, the river basin of Sundarban, is chosen due to its nature of water bodies such as wide rivers, narrow water streams, and sediment–water. The algorithm works with minimum human interaction. The method is validated by applying on Sentinal-2 and WorldView-2 images having a spatial resolution of 10 m and 0.46 m, respectively, and is found the accuracy is 97%.

Keywords Water body identification · Remote sensing · Histogram of gradient · NDWI

1 Introduction

Urban and rural water bodies transform their shape due to the effect of change in climate and environment. Natural calamities and constructions due to urban civilization are also liable for the change [1]. Water bodies such as rivers, reservoirs, and large lakes often change their routes and become a cause of floods and natural disasters [34]. These are also the primary sources of water supply in nearby cities or urban areas. A rapid change in such water resources needs to be detected timely [2]. As a result, it becomes necessary to identify and segregate water bodies to track natural and human-made water resources. Recent advancements in remote sensing and its advantages such as broader coverage and faster processing have made it easier in water detection. This technology is also efficient and used in extracting water areas from a large and complex geographical coverage [3,4].

Water body detection methods are supervised, unsupervised, and index based. In the foremost category, the analysis is on spectral characteristics of individual bands [5]. Decision tree [6], maximum likelihood analysis [7], artificial neural network (ANN) [8], and support vector machine (SVM) [9] are few applications of supervised learning. In the unsupervised category [36], K-means [10], iterative self-organizing

✉ Somnath Mukhopadhyay
som.cse@live.com

Tanmoy Halder
tanmoyhalder@gmail.com

Debasish Chakraborty
deba.isro@gmail.com

Ramen Pal
ramen.pal673@gmail.com

Sunita Sarkar
sarkarsunita2601@gmail.com

Nishtha Roy
nishtharoy1@gmail.com

Sunil Karforma
sunilkarforma@yahoo.com

1 Dr. B.C.Roy Engineering College, Durgapur, India

2 Department of Computer Science and Engineering, Assam University Silchar, Silchar, India

3 RRSC-East, NRSC, ISRO, Kolkata, India

4 Department of Computer Science, Burdwan University, Burdwan, India

Published online: 24 November 2021

data analysis (ISODATA), and FCM [11] are mostly applied [12,13]. The latter one is our area of interest in the present study. In the index-based category [37], information from individual bands is mathematically formulated to create more differences between water and non-water areas. The water index promotes water portions, whereas the vegetation index does the same for forests and greeneries. The normalized difference water index (NDWI) [14] proposed by McFeeters is widely being used for decades to identify surface water. NDWI is less complex to implement, and the accuracy level is also up to the mark. In 2013, this index was applied with a threshold of 0.3 for individual pixels to detect water pixels [15]. Xu in 2006 modified the existing NDWI method and improved the accuracy rate in urban areas by using the mid-infrared band rather than green and near-infrared bands [16]. This modification over NDWI is known as modified NDWI (MNDWI). Noise like the reflection of building shadows frequently matches the spectral reflectance of water bodies. [17]. Feyisa et al. [18] modified NDWI to distinguish water from shadows. Their proposal used two different automated water index (AWEI) methods, AWEI_{nsh} and AWEI_{sh}. The latter one not only separates water but also removes shadows. A simple enhanced water index (EWI) has been proposed by Wang et al. [19] which can identify information about water pixels using water surface proportion in inland river basins. Rokni et al. [20] compared different indexes and showed that NDWI identifies water better than MNDWI, normalized difference moisture index (NDMI) [21], water ratio index [22], and AWEI. Normalized difference vegetarian index (NDVI) was introduced for vegetation and greeneries [23]. Water identification index was combined with color space transformation and achieved more accuracy by removing noise [24]. In their proposal, Hao et al. identified surface water from Panjiakou Reservoir (China) [25]. Indexes such as NDWI, MNDWI, and AWEI_{nsh} are applied over a segmented MS image after an atmospheric correction. The work of [20] on Lake Urmia (Iran) detected the change in the lake region. To evaluate the proposal, NDWI, MNDWI, NDMI, and AWEI are applied on a series of Landsat images. [26] used urban water index (UWI) and urban shadow index (USI) to extract water from MS images. Spectral analysis of high-resolution images and linear SVM was used to establish UWI and USI. However, the performance of this method heavily depends on the atmospheric correction of data.

In 2017, the study of Gulcan et al. on Lake Burdur detected the change in the water body of the lake. Structural similarity index measure (SSIM) was applied to verify the accuracy of AWEI, NDWI, and MNDWI [27]. In 2018, the study of Acharya et al. on NDWI showed that solely NDWI or NDVI could not remove snow and shadows, whereas a combination of NDWI, NDVI, and AWEI improves the accuracy [28]. A study on Fengyun-3 medium resolution spectral imager data identified surface water of Poyang Lake (China) using seven different methods [29]. E. Ozelkan proposed that the NDWI using the Green-NIR is most accurate than Green-SWIR1 and Green-SWIR2. The work carried out on Landsat-8 OLI image of different lakes [30]. In recent work, the textural feature of entropy in a Sentinal-2 image has been used to detect surface water. For classification of MS image, K-means has been applied and mapped with the entropy textural image to identify water.

Statistical features like the gradient of different surfaces on earth are dissimilar in a remote sensing image. This identifying can be applied to separate water from other surfaces. Normally, a gradient in a digital image shows the change in image intensity. As water has comparatively more minor variation than other surfaces on earth, fewer pixels fall on the edges [35]. Pixels that belong to the water body in an MS image have similar intensity values or differ in a minimum. On the other hand, rocks, greeneries, and manufactured structures have variations in pattern. Pixels containing edges are more in numbers within those regions. In the present method, this observation was carried out using the gradient of pixels from individual clusters. A histogram of the gradient can reflect this observation statistically. However, very little research work has still been done now on the said application of features. The study of [31] has applied a textured pattern of entropy to fulfill the purpose of a Sentinel-2 image. In the present hybrid approach of water identification, a gradient is utilized. FCM is applied for classification, followed by cluster-wise calculation of NDWI. Therefore, gradient of individual clusters is observed to distinguish water regions from other surfaces. Salient findings in this study are: (1) a bi-way approach of water body detection; (2) application of gradient to distinguish water from other surfaces; (3) a dynamic threshold-based identification of water pixels; and (4) engagement of minimum bands during the process; only red, green, and NIR band is used where non-availability of other bands like SWIR could be overlooked.

The rest of the paper is organized as follows. Section 2 discusses the study area; a discussion on FCM and NDWI is presented in Sect. 3; Sect. 4 is all about methodology, followed by result analysis and discussion in Sect. 5, whereas Sect. 6 concludes the study.

2 Study area

Sundarban is the world's largest delta area formed by the River Ganges. A portion is located in the state of West Bengal, India, and the rest in Bangladesh. The total area is around 1330 sq. km (21°50'17" N, 88°53'07" E). The area is famous for its wildlife ecosystem, backwater, and mangroves. We selected this area for study due to its variety of water bodies such as wide rivers, narrow streams of flooded water, lakes/ponds made of the backwater, and sediment–water. Fig-

ure 3 shows a 10-m resolution Sentinel-2 view of the study area with three bands, which is used in the present study for the experiment.

3 Preliminaries

3.1 Fuzzy c-means (FCM)

The logic of the fuzzy set influences this unsupervised clustering algorithm. In 1973, the clustering mechanism of FCM was developed by J.C. Dunn [11], and further, it was improved by J.C. Bezdek [32]. The mean of all the points within a cluster is the centroid of that cluster. For any point x, of kth cluster with a weight w, cluster center is calculated using Eq. 1.

$$c_k = \frac{\sum_x w_k(x)^m x}{\sum_x w_k(x)^m} \tag{1}$$

where m is the influence parameter of the weights. The objective parameter in FCM could be written using Eqs. 2 and 3.

$$J = \sum_{j=1}^{k} \sum_{i=1}^{n} w_{i,j}^m \| x_i - c_j \|^2 \tag{2}$$

where

$$w_{ij} = \frac{1}{\sum_{k=1}^{c} (\frac{\|x_i - c_j\|}{\|x_i - c_k\|})^{\frac{2}{m-1}}}. \tag{3}$$

X is a finite set of n elements where $X = x_1, x_2, \ldots, x_n$. Outcomes of FCM are a list of c cluster centers. $C = c_1, c_2, \ldots c_c$ along with a partition matrix.

3.2 Water body indices

Normalized difference water index has widely been used in remote sensing to highlight water bodies from other earth surfaces. It is known for the simplicity of the method. The index is established on the fact that the water body absorbs the NIR band most and vegetarian reflects the NIR maximum [14,15]. It is presented in Equation 4.

$$\text{NDWI} = \frac{\text{GREEN} - \text{NIR}}{\text{GREEN} + \text{NIR}}. \tag{4}$$

4 The proposed method

A hybrid approach has been proposed here to extract water bodies from MS images. The methodology is based on the following three processes:

1. FCM is used for the classification of the MS image.
2. A dynamic threshold of NDWI is calculated to segregate clusters representing water and non-water.
3. Gradient is used for a second-order classification of water and non-water.

The proposed methodology is presented in Fig. 1. It starts with image segmentation using fuzzy c-means, followed by modified threshold calculation. The steps are discussed in the following subsections.

4.1 Dynamic threshold calculation

The threshold for NDWI is $\geq$ 0.3 [15]. Our study found that the value 0.3 always does not distinguish between water and non-water pixels. It depends on the number of clusters. Suppose there is a total of k pixels in a cluster. L_{NDWI} is calculated using Eq. 5.

$$L_{\text{NDWI}} = \frac{k}{\gamma} \tag{5}$$

where $\gamma = 2 + (n \times .1)$

Here, n is the number of clusters and γ is the *balancing factor*. Value of γ depends on the value of n [15]. It has been observed from experiments that the value of γ is directly proportional to n. That is, if n is higher, the value of γ will be increased. n is chosen by evaluating the best of the Davies–Bouldin index (DBI) and Silhouette score. If the number of pixels having NDWI value $\geq$ 0.3 for a cluster is $\geq l_{NDWI}$, then it is identified as water.

4.2 Image segmentation and histogram of gradient based for water body identification

Red, green, and NIR bands were selected for initial processing. A step-wise diagrammatic description is given in Fig. 1. This algorithm takes the input MS image and the total number of expected clusters as input. It generates the bi-thresholded (water body and non-water body) image as output. The detailed algorithm is as follows:

Step-1: Segment the input MS image into n number of clusters by using the FCM clustering algorithm.

Step-2: The segmented image is a 3D matrix of size P $\times$ Q $\times$ R, where P and Q indicate the total number of rows and columns in image and $R = 3$. Clusters are numbered as $c_1, c_2, \ldots c_n$.

Step-3: NDWI of the MS image is calculated using Eq. 4. The size of the NDWI image is P $\times$ Q $\times$ R, where $R = 1$.

Step-4: The clustered image is mapped against the NDWI image. Each cluster in the mapped image is marked as $Nd_1, Nd_2, \ldots Nd_n$.

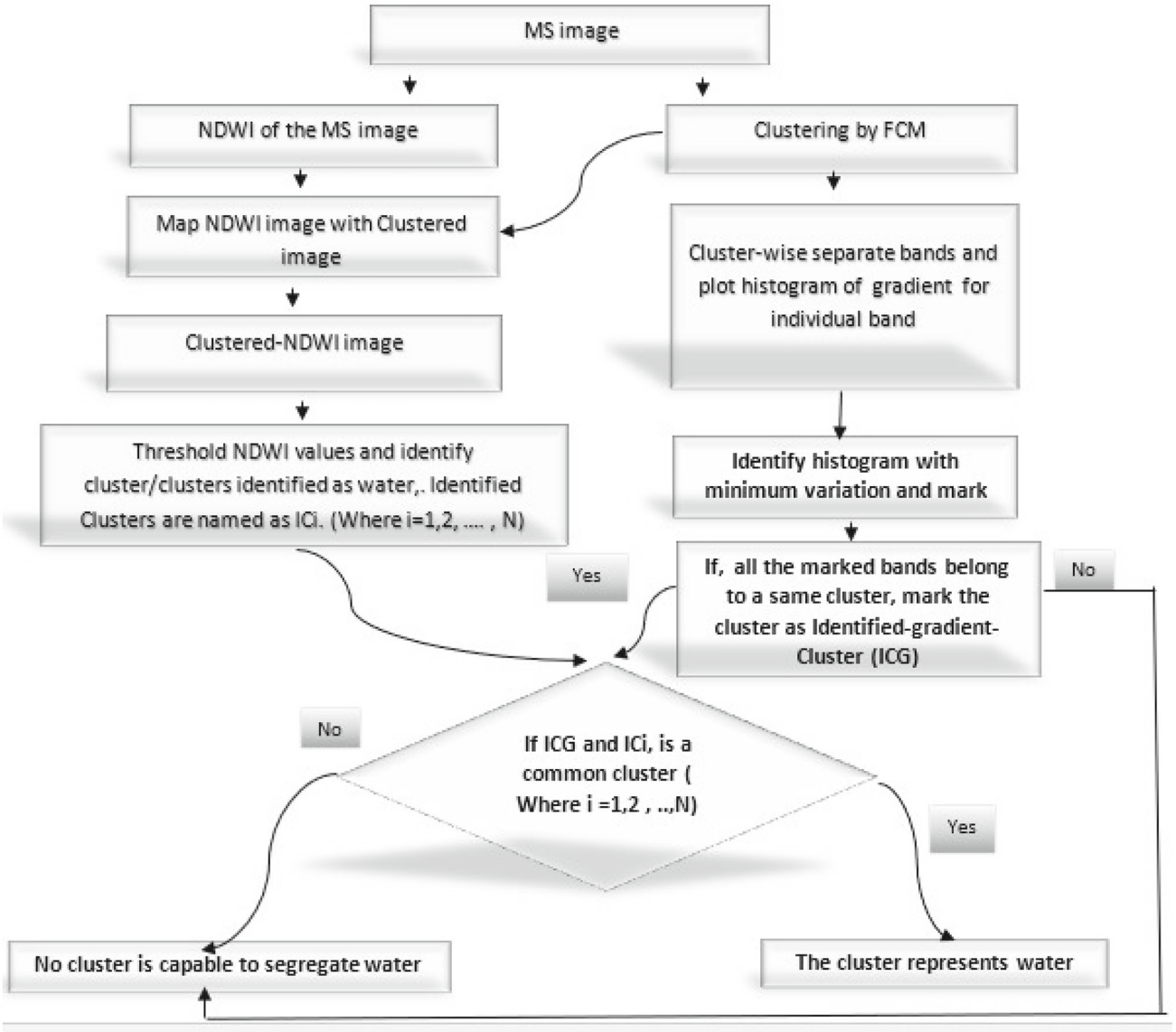

Fig. 1 Flowchart of the proposed method

Step-5: If the number of pixels having NDWI value ≥ 0.3 for c_i is $\geq l_{NDWI}$, then c_i is identified as water. l_{NDWI} is calculated by Eq. 5. There may be more than one cluster initially identified as water. The set of such clusters are IC_i, where $i = 0, 1, \ldots n$.

Step-6: Pixels are saved from each cluster in a $m \times 3$ matrix, where m denotes the number of rows. For n clusters, there are n matrices. Each $m \times 3$ matrix, corresponding to each c_i, is separated column wise and therefore denoted as $c_i r$, $c_i g$, and $c_i nir$.

Step-7: Cluster-wise histogram of the gradient is plotted. Equation 6 is used to calculate it for an individual cluster.

$$\nabla f(p) = \begin{Bmatrix} \frac{\delta f}{\delta x_1}(p) \\ . \\ . \\ . \\ \frac{\delta f}{\delta x_N}(p) \end{Bmatrix}. \tag{6}$$

In Eq. 6, gradient denotes differentiable function (f) of a scalar value in the vector field ∇f at point p. Its components are partial derivatives. ∇ denotes a vector differential operator.

(a) Worldview-2 image of Sundarban river basin. The study area is highlighted in red.

(b) Closed view of the study area highlighted in image 2(a)

(c) Closed view of the study area

Fig. 2 Dataset of Sundarban river basin, West Bengal, India: **a** WorldView-2 image of Sundarban river basin. **b** Closed view of the study area. **c** Zoomed view of the study area

Step-8: $Min(Gc_ir, Gc_ig, Gc_inir)$ is identified [where Min means histogram having minimum variation in graph]. If $Min(Gc_ir, Gc_ig, Gc_inir)$ for all ci belongs to a particular cluster, initially the cluster is marked and named as (ICG).

Step-9: $If\, ICG \cap ICi$ indicates a common cluster, it concludes that the identified cluster represents water.

5 Results and discussion

This section shows and analyzes results obtained from the present proposal and other cutting edge methods such as McFeeters et al. [15], Xu et al. [16], Dev et al. [28], and Ovakoglou et al. [31]. All the experiments are done in Python programming language in a system with the Intel i3 processor having 8 GB of RAM.

Figure 2a is the WorldView-2 image of the Sundarban river basin. The study area is highlighted in red. Figure 2b shows the closed view of the study area. The study area is highlighted in yellow. A zoomed view of the study area is shown in Fig. 2d.

Figure 3 is the Sentinel-2 view of the study area used in the current study for the experiment. In Fig. 4, surface water in other index-based studies is arranged as follows: 4(a) McFeeters et al. [15], 4(b) Xu et al. [16], 4(c) Dev et al. [28], and 4(d) Ovakoglou et al. [31]. In Ovakoglou et al. [31], entropy textural analysis and automatic detection of the threshold have been used. In Figs. 5 and 6, results obtained from the present study are shown. Figure 5a is the clustered image of the study area (Fig. 3). Water is highlighted in

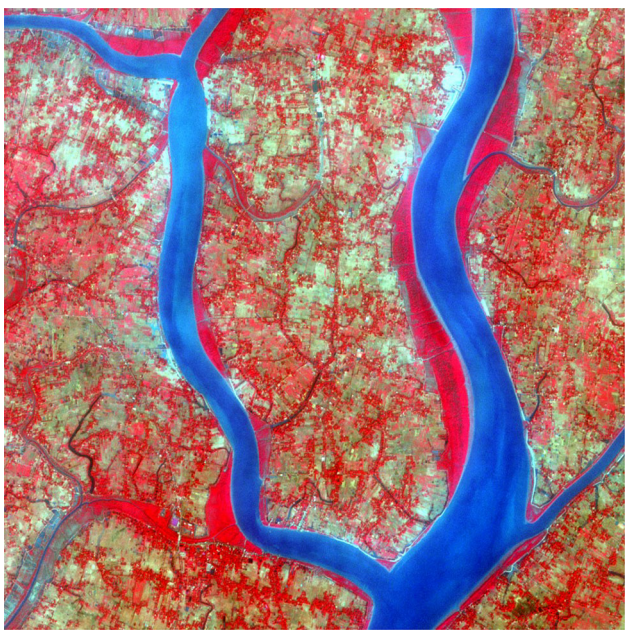

Fig. 3 Sentinel-2 view of the study area from Sundarban river basin. Picture taken on April 2020. Blue color represents surface water in the image

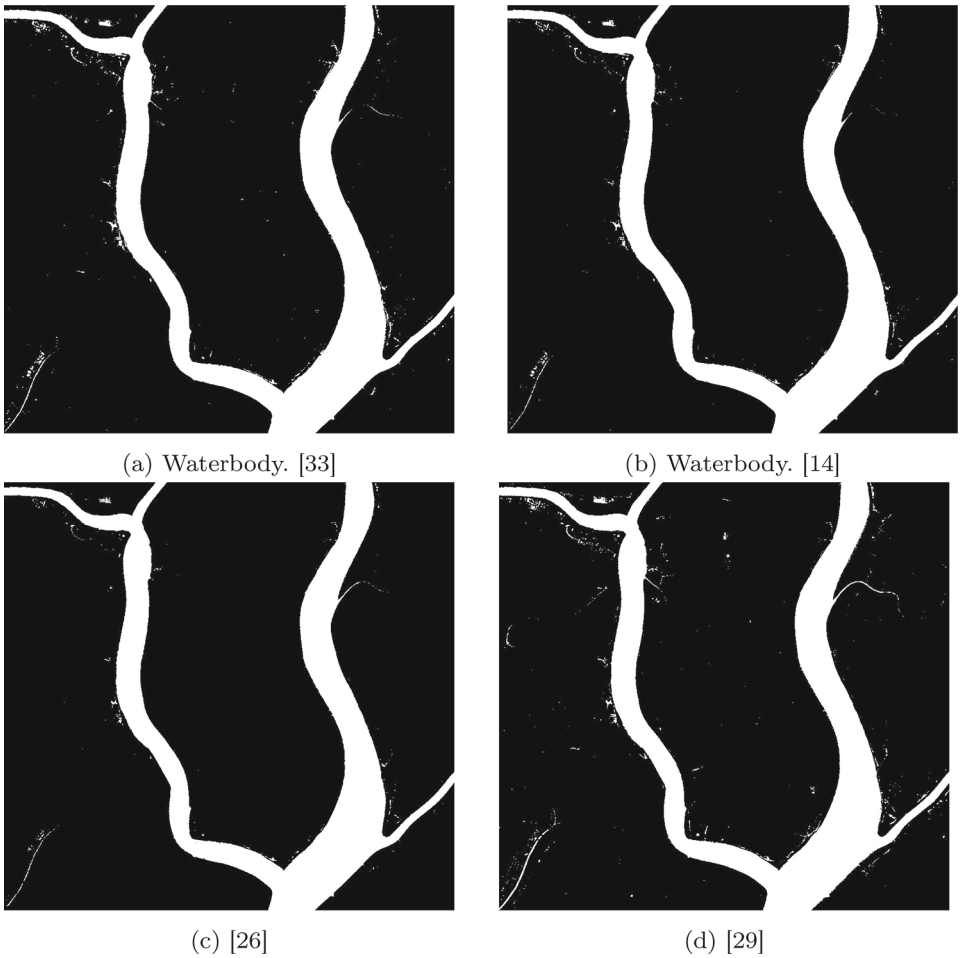

(a) Waterbody. [33] (b) Waterbody. [14]

(c) [26] (d) [29]

Fig. 4 **a** Surface water identified by McFeeters et al. [15]. **b** Surface water identified by Xu et al. [16]. **c** Surface water by Dev et al. [28] and **d** surface water by Ovakoglou et al. [31]

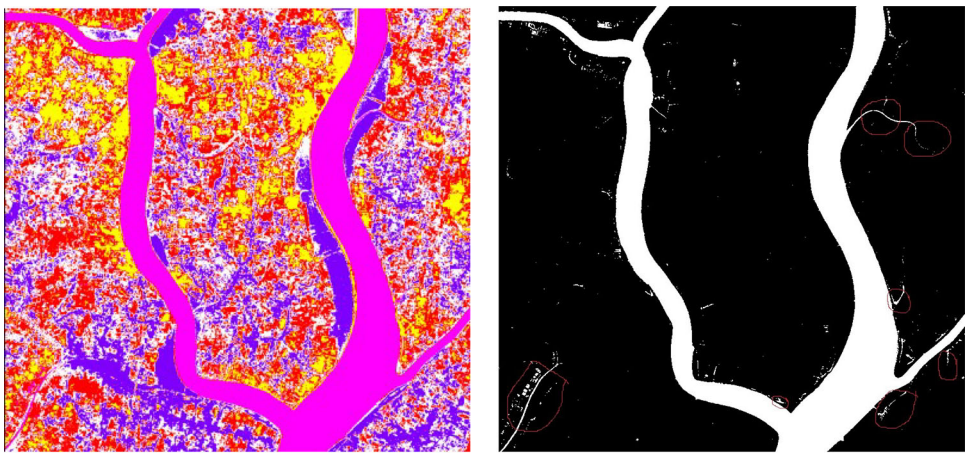

(a) Clustered image of figure 3 (b) Surface water using the current study

Fig. 5 **a** Clustered image of Fig. 3. **b** Surface water with true positives using the current study

pink. Here, in the experiment, five clusters have been used. The Davies–Bouldin index (DBI) observed in the experiment is 0.53, and the Silhouette score is 0.69. Figure 6 shows band-wise histogram observed for individual clusters. From visual observation of histograms cluster, 3 has the lowest variation in gradient. Hence, from feature-based analysis, cluster 3 is surface water. NDWI-based mapping also indicates that cluster 3 represents surface water. Surface water used in the present study is shown in Fig. 5b. A narrow stream of water and sediment–water is more clearly visible in the figure when compared with other index-based water identification methods in Fig. 4. Noticeable areas encircled in red in Fig. 5b

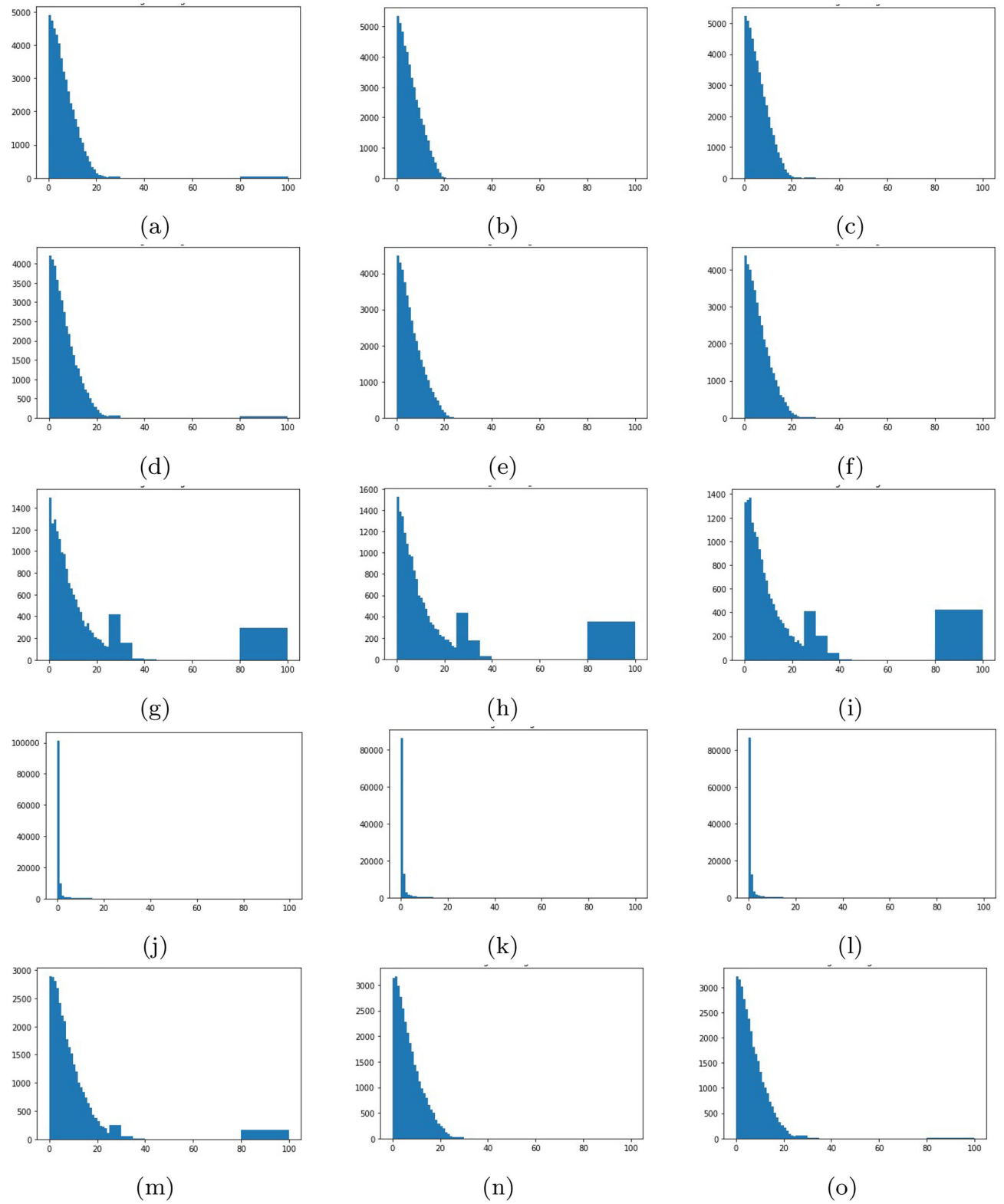

Fig. 6 Histogram of gradients of image 3. Each row represents a cluster, numbered from 0 to 4. Each column represents a band, numbered from 1 to 3

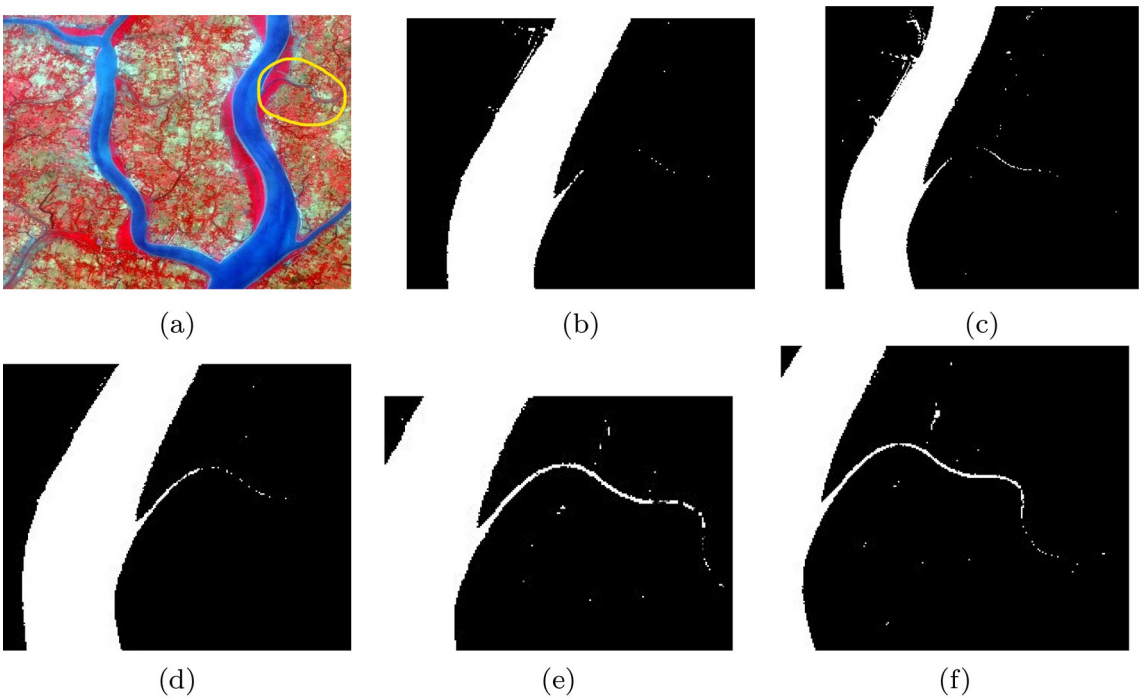

Fig. 7 **a** Narrow water stream encircled in yellow. Closed view of the encircled area highlighting surface water from the narrow stream using proposals of **b** McFeeters et al. [15], **c** Xu et al. [16], **d** Dev et al. [28], **e** Ovakoglou et al. [31], and **f** the present study

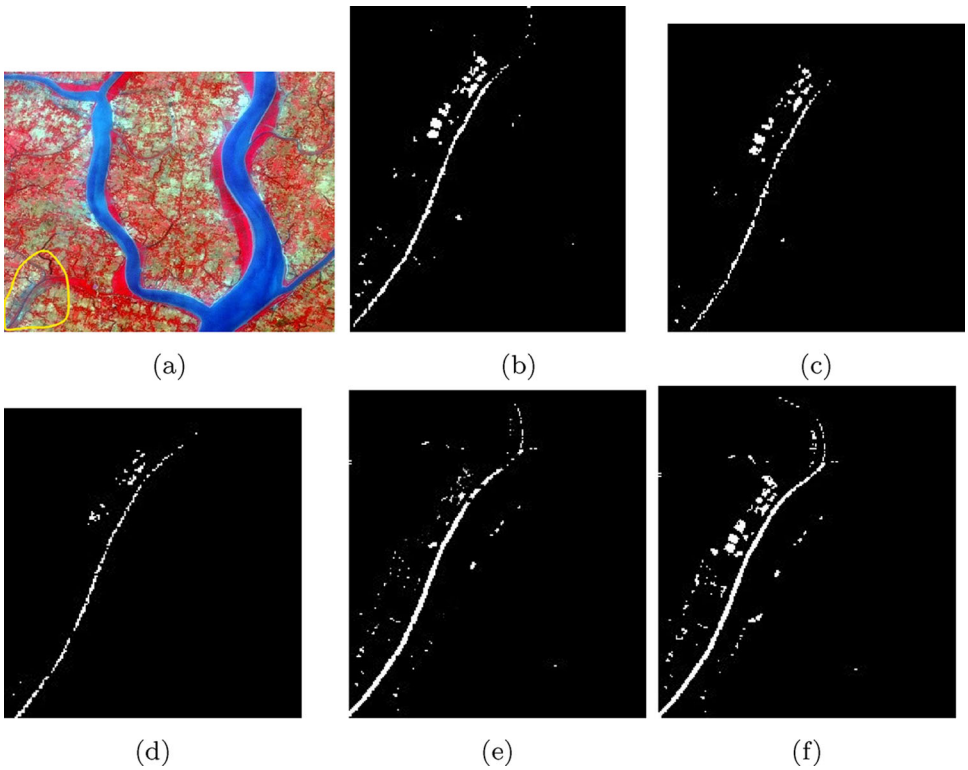

Fig. 8 **a** Sediment–water and narrow water stream encircled in yellow. Closed view of the encircled area highlighting sediment–water from the narrow stream using proposals of **b** McFeeters et al. [15], **c** Xu et al. [16], **d** Dev et al. [28], **e** Ovakoglou et al. [31], and **f** the present study

Fig. 9 Ground-truth regions

Table 1 The confusion matrices showing the classification accuracy obtained by the proposed hybrid approach

Actual class	Interpreted class Water	Non-water	Row total	Classification accuracy(%)	$C(\%)$	$O(\%)$
Water	676	13	689	96.84	3.15	1.86
Non-water	22	728	750	92.63	1.75	2.97
Column total	698	741	1439			

are sediment–water and narrow streams, which are better visible in the image. Figures 7 and 8 show a closed-view from image 5(b), where sediment–waters and narrow water streams are more prominently observed. For comparison, a closed view of McFeeters et al. [15], Xu et al. [16], Dev et al. [28], and Ovakoglou et al. [31] is also shown in Fig. 8. Table 1 covers water and non-water regions. ERDAS/IMAGINE software was used for digitizing the ground-truth regions. The digitized data are overlaid in Fig. 9. The digitized data covering water bodies are marked as 1, 2, 3, and 4. In contrast, the digitized data covering non-water regions are marked as 5, 6, and 7 in the figure using the digitized data overlaid separately on the resultant outputs obtained from proposed clustering methods. The classification accuracies for the proposed approach are shown through confusion matrix [37]. The confusion matrices (Table 1) showed the accuracy of classifying water and non-water areas (94.58% and 92.63%, respectively) by the proposed method.

After close observation and comparison, we found that single indexing like McFeeters et al. [15] and Xu et al. [16] is incapable of identifying such kind of surface water. However, the merged indexing of Dev et al. [28] may identify lakes in the snow mountain region, but sediment–water is not visible using the approach. The entropy-based approach Ovakoglou et al. [31] shows maximum visibility than the other three approaches. However, narrow water streams with sediment–water are maximum visible in Figs. 7f and 8f than the other four methods mentioned in the study.

6 Conclusion

This automated, hybrid water identification method is a new dimension in surface water detection from MS images. In this research, we have made known that index-based approaches can identify rivers, but sediment–water of narrow streams is not prominently visible. A dynamic threshold overcomes misclassification of water pixels during clustering. The histogram analysis of gradient removes non-water clusters, if any. During the process, minimum numbers of bands (R, G, NIR) are involved in the algorithm. In this study, results are compared with current index-based surface water identification methods and two traditional index-based approaches. As a study area, the Sundarban river basin has been used herein the experiment where narrow backwater streams and sediment–water are challenging to identify from MS image. The proposed method yields good results when applied to an MS Sentinel-2 image with a spatial resolution of 10 m. In high-resolution multispectral images with a spatial resolution of 0.46 m, the approach was also found to be useful in identifying water bodies. In our future work, our motive is to involve more features other than the gradient to fulfill the purpose in a MS image.

References

1. Fletcher TD, Andrieu H, Hamel P (2013) Understanding, management and modeling of urban hydrology and its consequences for receiving waters: A state of the art. Adv. Water Res. 51:261–279
2. Wolski P, Murray-Hudson M, Thito K, Cassidy L (2017) Monitoring flood extent in large data-poor wetlands using MODIS SWIR data. Int J. Appl Earth Obs. 57:224–234
3. Byun Y, Han Y, Chae T (2015) Image fusion-based change detection for flood extent extraction using bi-temporal very high resolution satellite images. Remote Sens. 7:10347–10363
4. Yang X, Zhao S, Qin X, Zhao N, Liang L (2017) Mapping of Urban Surface Water Bodies from Sentinel 2 MSI Imagery at 10 m Resolution via NDWI-Based Image Sharpening. Remote Sens. 9:596
5. National Research Council. Integrating Multiscale Observations of U.S. Waters; The National Academies Press: Washington, DC, USA (2008)
6. Wu Xindong, Kumar Vipin, Ross Quinlan J, Ghosh Joydeep, Yang Qiang, Motoda Hiroshi, McLachlan Geoffrey J, Ng Angus, Liu Bing, Yu Philip S (2008) Zhou, Zhi-Hua. Top 10 algorithms in data mining. Knowledge and Information Systems. 14 (1): 1-37
7. Rossi Richard J (2018) Mathematical Statistics: An Introduction to Likelihood Based Inference. New York: John Wiley and Sons. p. 227. ISBN 978-1-118-77104-4

8. McCulloch Warren, Pitts Walter (1943) A Logical Calculus of Ideas Immanent in Nervous Activity. Bulletin of Mathematical Biophysics. 5(4):115–133
9. Cortes Corinna, Vapnik Vladimir N (1995) Support-vector networks. Machine Learning. 20(3):273–297
10. MacQueen JB (1967) Some Methods for classification and Analysis of Multivariate Observations. Proceedings of 5th Berkeley Symposium on Mathematical Statistics and Probability. 1. University of California Press., pp. 281-297
11. Dunn JC (1973) A Fuzzy Relative of the ISODATA Process and Its Use in Detecting Compact Well-Separated Clusters. Journal of Cybernetics 3(3):32a57. https://doi.org/10.1080/01969727308546046
12. Lu D, Weng Q (2007) A survey of image classification methods and techniques for improving classification performance. Int. J. Remote Sens. 28:823–870
13. Otukei J, Blaschke T (2010) Land cover change assessment using decision trees, support vector machines and maximum likelihood classification algorithms. Int. J. Appl. Earth Obs. Geoinf. 2010(12):S27–S31
14. McFeeters S (1996) The use of the Normalized Difference Water Index (NDWI) in the delineation of open water features. Int. J. Remote Sens. 17:1425–1432
15. McFeeters SK (2013) Using the Normalized Difference Water Index (NDWI) within a Geographic Information System to Detect Swimming Pools for Mosquito Abatement: A Practical Approach. Remote Sens. 5(7):3544–3561
16. Xu H (2006) Modification of normalised difference water index (NDWI) to enhance open water features in remotely sensed imagery. Int. J. Remote Sens. 27:3025–3033
17. Niroumand-Jadidi M, Vitti A (2017) Reconstruction of river boundaries at sub-pixel resolution: Estimation and spatial allocation of water fractions. ISPRS Int. J. Geo-Inf. 6:383
18. Feyisa GL, Meilby H, Fensholt R, Proud SR (2014) Automated Water Extraction Index: A new technique for surface water mapping using Landsat imagery. Remote Sens. Environ. 140:23–35
19. Wang S et al (2015) "A Simple Enhanced Water Index (EWI) for Percent Surface Water Estimation Using Landsat Data," in IEEE Journal of Selected Topics in Applied Earth Observations and Remote Sensing, vol. 8, no. 1, pp. 90-97, Jan. 2015, https://doi.org/10.1109/JSTARS.2014.238719
20. Rokni K, Ahmad A, Selamat A, Hazini S (2014) Water Feature Extraction and Change Detection Using Multitemporal Landsat Imagery. Remote Sens. 6:4173–4189
21. Wilson EH, Sader SA (2002) Detection of forest harvest type using multiple dates of Landsat TM imagery. Remote Sens. Environ. 2002(80):385–396
22. Shen L, Li C (2010) Water Body Extraction from Landsat ETM+ Imagery Using Adaboost Algorithm. In: Proceedings of 18th International Conference on Geoinformatics, 18-20 June 2010, Beijing, China; pp. 1-4
23. Rouse JW, Haas RH, Schell JA, Deering DW (1973) Monitoring Vegetation Systems in the Great Plains with ERTS (Earth Resources Technology Satellite). In: Proceedings of Third Earth Resources Technology Satellite Symposium, Greenbelt, ON, Canada, Volume SP-351, pp. 309-317
24. Jiang Z, Qi J, Su S, Zhang Z, Wu J (2012) Water body delineation using index composition and HIS transformation. Int. J. Remote Sens. 33:3402–3421
25. Jiang H, Feng M, Zhu Y, Lu N, Huang J, Xiao T (2014) An Automated Method for Extracting Rivers and Lakes from Landsat Imagery. Remote Sens. 6:5067–5089
26. Wu W, Li Q, Zhang Y, Du X, Wang H (2018) Two-Step Urban Water Index (TSUWI): A New Technique for High-Resolution Mapping of Urban Surface Water. Remote Sens. 10:1704
27. Sarp Gulcan (2017) Mehmet Ozcelik (2017). Water body extraction and change detection using time series: A case study of Lake Burdur, Turkey, Journal of Taibah University forScience 11(3):381–391
28. Acharya TD, Subedi A, Lee DH (2018). Evaluation of Water Indices for Surface Water Extraction in a Landsat 8 Scene of Nepal. Sensors (Basel). 2018 Aug; 18(8): 2580.Published online 2018 Aug 7
29. Wei Xufeng, Wenbo Xu, Bao Kuanle, Hou Weimin, Jia Su, Li Haining, Miao Zhuang (2020) A Water Body Extraction Methods Comparison Based on FengYun Satellite Data: A Case Study of Poyang Lake Region. China. Remote Sens. 2020(12):3875. https://doi.org/10.3390/rs12233875
30. Ozelkan Emre (2020) Water Body Detection Analysis Using NDWI Indices Derived from Landsat-8 OLI. Pol. J. Environ. Stud. Vol. 29, No. 2 (2020), 1759-1769
31. Ovakoglou Georgios et al (2021) Automatic detection of surface-water bodies from Sentinel-1 images for effective mosquito larvae control. J. of Applied Remote Sensing 15(1):014507
32. Bezdek James C (1981) Pattern Recognition with Fuzzy Objective Function Algorithms. ISBN 0-306-40671-3
33. Canny J (1986) A Computational Approach To Edge Detection (1986). IEEE Transactions on Pattern Analysis and Machine Intelligence 8(6):679–698
34. Martin Ester, Kriegel Hans-Peter, Sander Jarg, Xu Xiaowei (1996) Simoudis, Evangelos; Han, Jiawei; Fayyad, Usama M. (eds.). A density-based algorithm for discovering clusters in large spatial databases with noise. Proceedings of the Second International Conference on Knowledge Discovery and Data Mining (KDD-96). AAAI Press. pp. 226231 (1996). ISBN 1-57735-004-9
35. Ji L, Zhang L, Wylie B (2009) Analysis of dynamic thresholds for the normalized difference water index. Photogramm. Eng. Remote Sens. 75:1307–1317
36. Tussupova K, Anchita Hjorth P, Moravej M (2020) Drying Lakes: A Review on the Applied Restoration Strategies and Health Conditions in Contiguous Areas. Water, 12, 749
37. Joseph G (2013) Fundamental of remote sensing, 2nd edn. Universities Press, India